

## THERMAL, MORPHOLOGICAL, AND DFT STUDIES ON THE SCANDIUM(III) SULFA DRUGS COMPLEXES

Abeer A. El-Habeeb<sup>1</sup>, Moamen S. Refat<sup>2</sup>, Q. Mohsen<sup>2</sup> and Kareem A. Asla<sup>3\*</sup>

<sup>1</sup>Department of Chemistry, College of Science, Princess Nourah bint Abdulrahman University, P.O. Box 84428, Riyadh 11671, Saudi Arabia

<sup>2</sup>Department of Chemistry, College of Science, Taif University, P.O. Box 11099, Taif 21944, Saudi Arabia

<sup>3</sup>Department of Chemistry, Faculty of Science, Zagazig University, Zagazig, 44519, Egypt

(Received February 27, 2025; Revised March 19, 2025; Accepted March 20, 2025)

**ABSTRACT.** Four scandium(III) sulfa drug complexes were studied based on thermal, kinetic, morphological and computational investigations. The isolated solid complexes were synthesized by 1:2 molar ratios between scandium(III) chloride and four kinds of sulfa drugs; **sulf-1** = sulfadimidine (**1**), **sulf-2** = sulfanilamide (**2**), **sulf-3** = sulfamethoxazole (**3**) and **sulf-4** = sulfadiazine (**4**). The molecular formulae for the isolated complexes are [Sc(**sulf-1**)<sub>2</sub>(Cl)<sub>2</sub>]Cl (**5**), [Sc(**sulf-2**)<sub>2</sub>(Cl)<sub>2</sub>]Cl (**6**), [Sc(**sulf-3**)<sub>2</sub>(Cl)<sub>2</sub>]Cl (**7**) and [Sc(**sulf-4**)<sub>2</sub>(Cl)<sub>2</sub>]Cl (**8**). TGA thermograms for complexes (**5-8**) were utilized to study the different degradation steps. Moreover, the kinetic and thermodynamic functions have been calculated based on the data speculated for compounds (**5-8**). The surface morphology of (**5-8**) was studied by scanning electron microscopy (SEM). The compounds (**5-8**) exhibit favorable crystallinity, as X-ray powder diffraction (XRD) confirmed. The nano-scale of the samples was confirmed by the transmission electron microscopy (TEM) images. Furthermore, the DFT calculations for (**1-8**) were performed. The bond lengths for (**5-8**) are reduced or increased rather than that of free drug molecules due to complexation. Bond angles of compounds (**5-8**) predict the octahedral geometry (Oh) of Sc(III). The calculated vibrational spectra for compounds (**5-8**) were compared to the experimental IR, which may give quite differences attributed to different phases of measurement.

**KEY WORDS:** Scandium, Sulfa-drugs, TGA, SEM, TEM, DFT, Coats-redfern, Complexes, Nano-particles

## INTRODUCTION

Sulfa drugs and their metal complexes, which often exhibit enhanced antibacterial and antifungal potency, have been extensively studied for applications in burn treatment, heavy metal ion interactions, and biological activities, as demonstrated by various researchers [1]. The biological activities of some metal sulfasalazine complexes were tested [2-4]. Marwa Hassan *et al.* reported the synthesis of some sulfa drug metal complexes. The synthesized compounds were tested to have enhanced therapeutic potential for the treatment of various types of infections and malignancies [5]. Rostamizadeh *et al.* synthesized and characterized different sulfamethoxazole and sulfabenzamide metal complexes. The analysis predicted more activity of sulfamethoxazole metal Zn(II) complexes than free drugs [6]. Afaf Bouchoucha *et al.* synthesized and thoroughly characterized some sulfamethoxazole metal complexes. Using the DFT approach, the structure of the metal complexes under study was optimized [7]. Al-Khodir synthesized sulfamethoxazole complexes with Ca<sup>2+</sup>, Zn<sup>2+</sup>, and Au<sup>3+</sup>. The compounds were in nanoscale and characterized by SEM, TEM and powder XRD. The antitumor efficacy of Au(III) complex have been tested [8]. DFT/B3LYP computational studies have been utilized to study the geometry and energy parameters for synthesized complexes derived from sulfa drug with some metal ions. Furthermore, the synthesized compounds were in the nanoscale as characterized XRD and TEM tools [9]. Sharfalddin *et al.* studied some transition metal complexes of sulfaclozine (SCZ).

\*Corresponding authors. E-mail: dr.kasla2020@gmail.com

This work is licensed under the Creative Commons Attribution 4.0 International License

Physicochemical studies were applied to elucidate the structure of the synthesized compounds. Moreover, computational studies have been applied using DFT method. The geometry optimization as well as energy parameters were in a good agreement with experimental data [10]. Abrar Ul Hassan and Shehnaz *et al.* prepared and studied the Schiff base complexation as well as DFT method was utilized to verify the geometry in addition, other energy parameters have been calculated [11, 12]. Nursel Açar *et al.* utilized the DFT method to optimize the geometry of sulfadiazine and sulfadiazine-cysteine compounds. The electron densities, and UV-Vis absorption spectra and other energy parameters have been calculated as well [13]. A series of lanthanide metal complexes with sulfonamide were reported. The experimental data are comparable data obtained by computational studies using DFT method [14]. Bouzaheur *et al.* synthesized sulfonamide Pd(II) and Pt(IV) metal complexes. The compounds investigated were characterized by different techniques and the results were compared by the theoretical data computed by DFT method [15]. Thiazole Schiff base metal complexes have been synthesized and characterized with different techniques. The compounds studied were optimized and different energy parameters have been calculated using DFT/B3LYP method [16]. The nanostructured sulfamethoxazole (SMX) metal complexes have been investigated to have good biological potency. The complexes studied were characterized by SEM and powder XRD [17]. Filiz Öztürk synthesised metal(II) sulfamethoxazole complex. The cadmium complex was optimized with DFT method and other energy descriptors were computed as well. Furthermore, Hirshfeld surface analysis and Molecular orbital coefficients have been computed [18, 19]. In this study, the thermal characterization of the prepared scandium(III) complexes was performed using TGA and DrTGA techniques. The surface morphology and the crystallinity of the complexes were checked based on the electron microscopes as well as XRD techniques, respectively.

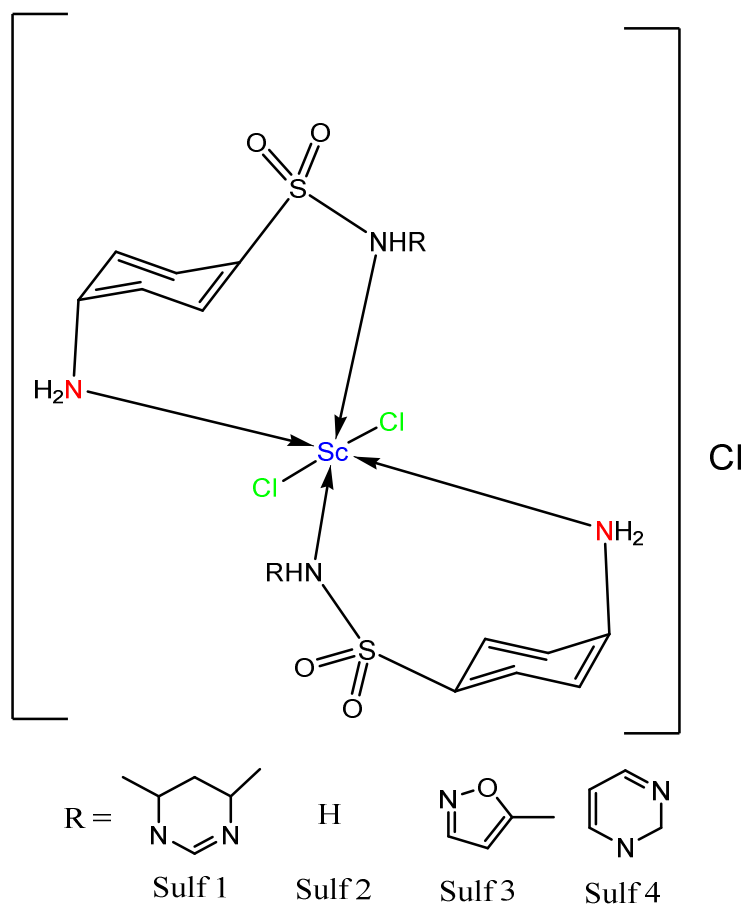
## EXPERIMENTAL

### *Synthesis of Sc(III) sulfa drug complexes*

The free sulfa-drugs (**1-4**) as well as scandium(III) chloride salt were purchased from Sigma-Aldrich Chemical Corporation. The chemicals were used without any additional purifications. The scandium(III) sulfa drugs complexes have been synthesized and characterized in our previous work [20]. The molecular formulae of synthesized compounds are [Sc(**sulf-1**)<sub>2</sub>(Cl)<sub>2</sub>]Cl (**5**), [Sc(**sulf-2**)<sub>2</sub>(Cl)<sub>2</sub>]Cl (**6**), [Sc(**sulf-3**)<sub>2</sub>(Cl)<sub>2</sub>]Cl (**7**), [Sc(**sulf-4**)<sub>2</sub>(Cl)<sub>2</sub>]Cl (**8**). All samples have been heated under N<sub>2</sub> gas to 800 °C using A Shimadzu thermo-gravimetric analyzer model (TG/DTG-50H). The surface images were obtained utilizing a scanning electron microscopy (SEM) model (specifically the Quanta FEG 250 instrument). The crystal structures were measured using the X-ray diffraction technique, model (X'Pert PRO PAN analytical XRD). The morphology and the particle size were recorded by the transmission electron microscopy (TEM) model (JEOL 100s microscopy).

### *Geometry optimization*

Computational investigations were conducted using the DMOL<sup>3</sup> software from the Materials Studio package [21]. These studies were performed utilizing double numerical basis sets and the polarization functional (DNP) for the DFT semi-core pseudopotentials (dspp) [22, 23]. The RPBE functional, based on the generalized gradient approximation (GGA) and known for its excellent correlation, was employed as the fundamental approach [24].



Scheme 1. Suggested structure formulae for Sc(III)-sulfa drugs complexes.

## RESULTS AND DISCUSSION

### *Thermo gravimetric analyses*

Figures 1 and 2 show TGA and DrTGA thermograms, respectively. The TGA degradation steps for compounds (1-4) Figure 1 and for (5-8) chelates Figure 2 have been tested under nitrogen gas up till 800 °C.

The DrTGA thermograms for free drugs (1-4) and for (5-8) chelates show that the decomposition occurs in two or three endothermic degradation steps. The degradation temperature ranges from (243-435 and 455-676 °C), (255-321, 324-392 °C and 400-630 °C) and (223-414 and 438-672 °C) for compounds 1, 2, 3, and 4, respectively. The mid temperatures ( $\text{DTG}_{\text{max}}$ ) corresponding to the maximum degradation for each step are (290.5 and 588), (298, 347 and 526 °C), (315 and 575 °C) and (282, 380 and 550 °C), respectively. Furthermore, the degradation

ranges from (244-369 and 427-597 °C), (200-396 and 475-668 °C), (206-369 and 480-660 °C) and (204-324, 330-428 and 466-636 °C) for chelates **5**, **6**, **7**, and **8**, respectively. The mid temperatures ( $DTG_{max}$ ) are (296 and 522), (271 and 493 °C), (311 and 561 °C) and (289, 367 and 556 °C), respectively. There are no leftover species at 800 °C, meaning the experiment's overall weight loss is 100%.

There are two degradation stages for complex **5** (Figure 2). One drug molecule and two chlorine molecules decompose during the first stage of decomposition. A 50.472% weight loss accompanies this stage due to the loss of one chlorine atom and another drug molecule. The second stage of disintegration results in a weight loss of 43.485%. The percentage found for the residue after the decomposition process is 6.043% due to scandium metal. As illustrated in (Figure 2), there are two stages in the thermal degradation of complex **6**. The dissociation of one drug molecule and a weight loss of 37.429% coincide with the initial stage of the decomposition. Because of the breakdown of additional drug molecules, the total weight losses at this stage are 35.147%.  $ScCl_3$  is the final product of thermal breakdown.

Two extremely strong endothermic degradation stages are involved in the heat degradation of complex **7** (Figure 2). The first stage of decomposition results in a weight loss of 29.654%, which corresponds to the loss of one drug molecule. The second thermal stage is characterized by a weight loss of 40.041%, which is equivalent to the loss of the second drug molecule. The residual 30.305% is equivalent to  $ScCl_3$  contaminated with few carbon atoms.

According to the TGA curve (Figure 1), compound **8** decomposes in three steps. The first mass loss is associated with the breakdown of one drug molecule (obs = 33.376%). The continuous second mass loss corresponds to eliminating three chlorine atoms (obs = 16.391%). The third stage's mass loss corresponds to the elimination of the second drug molecule, with a mass loss of 38.021%. The final decomposition product of complex **8** corresponds to  $\frac{1}{2}Sc_2O_3$  contaminated with few carbon atoms (obs = 12.212%).

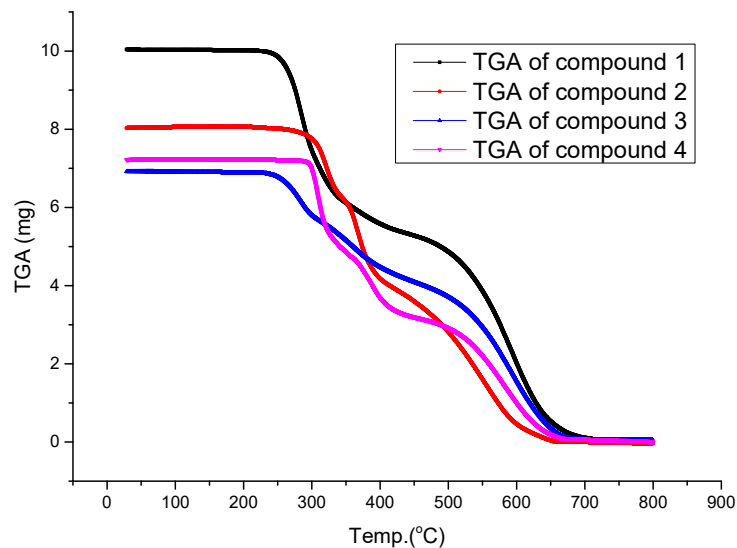


Figure 1. TGA curves of sulfa drugs (**1-4**).

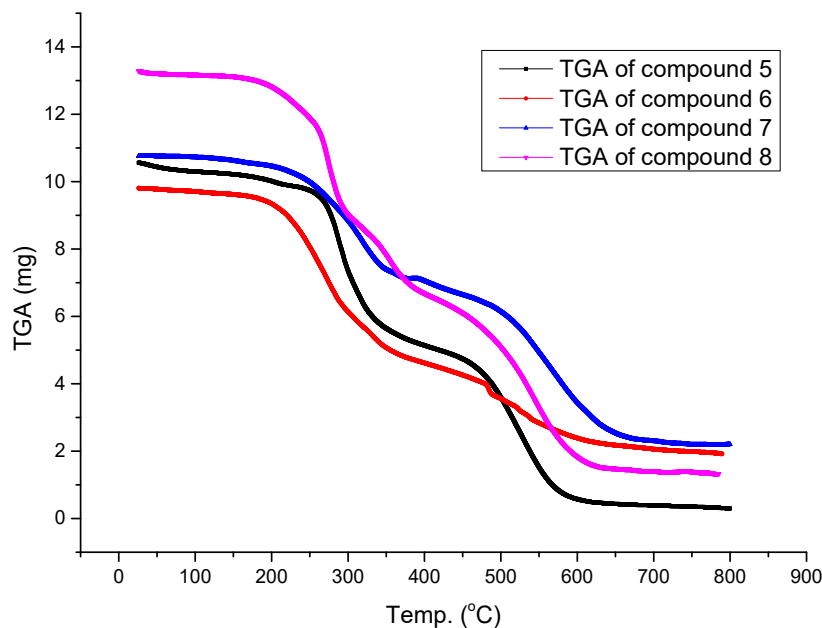


Figure 2. TGA for Sc-sulfa complexes.

#### Kinetic study

Tables 1 and 2 present the order ( $n$ ) and activation energy ( $E_a$ ) values for the different degradation stages of the compounds under investigation. The parameters were computed from TG and DTG thermograms using the Coats-Redfern and Horowitz-Metzger equations [25, 26]. The rate of the reaction is contingent upon both the decomposition temperature and the quantity of the sample. The following equation (1) describes the rate of degradation for a solid compound.

$$\frac{d\alpha}{dt} = K(T)g(\alpha) \quad (1)$$

In this case,  $\alpha$  represents the degree of change,  $T$  is the absolute temperature, and  $t$  is the time.

$$\alpha = \frac{w_0 - w_t}{w_0 - w_\infty} \quad (2)$$

The sample weights before degradation, at temperature  $t$ , and after entire conversion are denoted by  $w_0$ ,  $w_t$ , and  $w_\infty$ , respectively. The temperature-dependent function is denoted by  $K(T)$ , while the kinetic conversion function,  $g(\alpha)$ , can take on different functional forms. However, for solid-state reactions, its commonly used form is  $g(\alpha) = (1-\alpha)^n$ , where  $n$  represents the reaction order, which is presumed to be constant throughout the process [27, 28]. The Arrhenius Equation is typically used to express the rate constant (3):

$$k = A \exp\left(-\frac{E_a}{RT}\right) \quad (3)$$

$E_a$  denotes the activation energy;  $R$  represents the gas constant (J.K/mol), and the Arrhenius pre-exponential factor,  $A$ , represents the reaction rate. In Equation (2), substitution

$$\frac{d\alpha}{dt} = A \exp\left(-\frac{E_a}{RT}\right) g(\alpha) \quad (4)$$

Under a linear temperature schedule ( $T = T_0 + \beta t$ , where  $T_0$  is the starting temperature and  $\beta = dT/dt$  is the heating rate), the reaction occurs. It is also commonly recognized that the degradation is a first-order. The investigated entity's degradation processes were regarded as first-order reactions with ( $n=1$ ). Based on this presumption, equation (4) gives the following:

$$\ln(1-\alpha) = -\frac{A}{\beta} \int_{T_0}^T \text{Exp}\left(-\frac{E_a}{RT}\right) dT \quad (5)$$

Equation (5) makes it possible to use the integral approach to analyze empirical data and determine the degradation kinetic parameters  $A$  and  $E_a$ . The right-hand side of the equation's temperature integral has no exact analytical answers; hence different approximations are used. Two approaches that use various strategies to solve Equation (5) using the TGA data of the complexes under study are compared. These methods are:

#### *Coats-Redfern method*

The Coats-redfern [25] method is as follows:

$$\ln X = \frac{\ln\left[\frac{1-(1-\alpha)^{1-n}}{T^2(1-n)}\right]}{\ln\left(\frac{AR}{\beta E}\right) - \frac{E_a}{RT}} \quad \text{for } n \neq 1 \quad (5a)$$

$$\ln X = \frac{\ln\left[\frac{-\ln(1-\alpha)}{T^2}\right]}{\ln\left(\frac{AR}{\beta E}\right) - \frac{E_a}{RT}} \quad \text{for } n=1 \quad (5b)$$

$\ln X$  was plotted against  $1/T$  for the studied compounds. The correlation coefficient,  $r$ , was calculated using the least squares approach for a range of values of  $n$  ( $n=0, 0.33, 0.5, 0.66$ , and  $n=1$ ). The order parameter for the decomposition step of interest was determined to be the value of  $n$  that produced the best fit (with  $R^2 \approx 1$ ). The intercept yields  $A$ , and the straight-line slope corresponds to ( $E_a/R$ ). Table 1 displays the gathered data.

#### *Horowitz-Metzger method [26]*

$$\ln[-\ln(1-\alpha)] = \frac{E_a \theta}{RT_s^2} \quad \text{for } n=1 \quad (5c)$$

$$\ln\left[\frac{1-(1-\alpha)^{1-n}}{1-n}\right] = \ln\left(\frac{A}{\beta} \frac{RT_s^2}{E}\right) - \frac{E_a}{RT_s} + \frac{E_a \theta}{RT_s^2} \quad \text{for } n \neq 1 \quad (5d)$$

$\theta$  is the difference between  $T_s$  (the peak temperature of the DTG) and  $T$  (the temperature correlated with weight loss,  $W_t$ ). With this method, the left-hand sides of Equations 5c and 5d plotted versus  $\theta$  should show a linear relationship with a slope of  $E_a/RT_s^2$ . Table 2 contains a record of the displayed data.

*Thermodynamic parameters*

The following Eyring [27] Equations (4-6) were utilized to compute thermodynamic parameters of activation:

$$\Delta H^* = E_a - RT \quad (6)$$

$$\Delta S^* = R \ln \frac{hA}{K_B T} \quad (7)$$

$$\Delta G^* = \Delta H - T\Delta S \quad (8)$$

The entropy, enthalpy of activation, and Gibbs free enthalpy of activation are represented by the variables  $\Delta H^*$ ,  $\Delta S^*$ , and  $\Delta G^*$ , respectively. They are expressed in kJ/mol, kJ/molK, and kJ/mol, respectively. The Planck and Boltzmann constants are denoted by the constants  $h$  and  $K_B$ , respectively. Tables 1 and 2 lists the kinetic parameters determined by combining the Horowitz-Metzger and Coats-Redfern techniques. Examining these two sets of kinetic parameters together shows no significant distinction in the approximations used in the Horowitz-Metzger method.

The following observations can be speculated from Tables 1 and 2. i) All decomposition steps are best fitted with higher correlation ( $R^2$ ) for  $n = 1$ . ii) For the subsequent degradation, the moiety's stability is indicated by the comparatively large activation energy or  $E_a$ . Since compounds **5** and **7** complexes have covalent bond characteristics, their  $E_a$  values are significantly greater than those of compounds **1** and **3**, respectively, indicating a high degree of stability [25]. In Tables 1 and 2, the total activation energy values were calculated, and it was shown that the metal complexes with the lowest thermal stability are in the order: of complex **8** > complex **5** > complex **7** > complex **6**. iii) For all the decomposition steps, the -ve sign of the entropy change ( $-\Delta S^*$ ) indicates the highly ordered fragments and the ( $+\Delta S^*$ ) suggests the randomness of the fragments. In addition, it suggests a slow rate of decomposition [26]. iv) The +ve sign of enthalpy of activation ( $+\Delta H^*$ ) predicts that thermal energy is necessary for the decomposition process. v) The sharp increase in positive values of the free energy of activation ( $+\Delta G^*$ ) predicts the non-spontaneity of the decomposition steps. Furthermore, the end residue has greater free energy than the starting molecule. The increase in  $T\Delta S^*$  values predict the stiffness of the remaining entity. Otherwise, the remaining moiety requires longer time and more energy to rearrange before it is given off [28-33].

Table 1. Kinetic parameters for sulfa drugs and their Sc-complexes assessed using the Coats-Redfern equation.

Compound	Peak	Mid temp (K)	$E_a$ kJ/mol	$A$ ( $S^{-1}$ )	$\Delta S^*$ kJ/mol.K	$\Delta H^*$ kJ/mol	$\Delta G^*$ kJ/mol
<b>1</b>	1 <sup>st</sup>	563.55	166.5066	2.74E+13	7.033779	161.821	157.8573
	2 <sup>nd</sup>	861.43	142.7191	3.21E+06	-129.166	135.557	246.8246
<b>2</b>	1 <sup>st</sup>	571.69	342.4796	1.22E+27	268.2032	337.726	184.3974
	2 <sup>nd</sup>	620.63	111.3653	1.52E+05	-151.803	106.205	200.4189
	3 <sup>rd</sup>	799	114.9303	5.05E+08	-86.502	108.287	177.4025
<b>3</b>	1 <sup>st</sup>	588	120.3728	1.80E+09	-73.371	115.484	158.6263
	2 <sup>nd</sup>	848.42	122.1868	2.13E+05	-151.62	115.133	243.7702
<b>4</b>	1 <sup>st</sup>	555.65	461.0609	1.55E+41	538.4333	456.441	157.2607
	2 <sup>nd</sup>	653.93	202.9635	3.66E+14	27.35376	197.526	179.6393
	3 <sup>rd</sup>	823.77	153.8966	3.00E+07	-110.219	147.047	237.8427
<b>5</b>	1 <sup>st</sup>	569	196.0188	1.48E+16	59.24887	191.288	157.5755
	2 <sup>nd</sup>	795	156.9978	1.17E+08	-98.5766	150.388	228.7565
<b>6</b>	1 <sup>st</sup>	544.75	72.15308	3.27E+04	-163.506	67.6240	156.6937

7	2 <sup>nd</sup>	766.18	101.9429	2.51E+66	1018.371	95.5728	-684.683
	1 <sup>st</sup>	584.31	65.8899	4.83E+03	-179.987	61.0319	166.2004
	2 <sup>nd</sup>	834.76	174.3262	8.48E+08	-82.5489	167.386	236.2946
8	1 <sup>st</sup>	562.59	60.30551	2.46E+03	-185.259	55.6281	159.8532
	2 <sup>nd</sup>	640	164.1637	1.85E+11	-35.5614	158.842	181.6021
	3 <sup>rd</sup>	829.39	144.6712	6.92E+06	-122.47	137.775	239.351

Table 2. Kinetic parameters for sulfa drugs and their Sc-complexes assessed using the Horowitz-Metzger equation.

Compound	Peak	Mid temp (K)	E <sub>a</sub> (kJ/mol)	A (S <sup>-1</sup> )	ΔS* (kJ/mol.K)	ΔH* (kJ/mol)	ΔG* (kJ/mol)
1	1 <sup>st</sup>	563.55	179.2853	2.41E+15	44.24805	174.6	149.664
	2 <sup>nd</sup>	861.43	185.5786	8.06E+09	-64.086	178.4166	233.6222
2	1 <sup>st</sup>	571.69	305.42	6.72E+26	263.2542	300.667	150.1672
	2 <sup>nd</sup>	620.63	92.03697	2147009	-129.793	86.87705	167.4304
	3 <sup>rd</sup>	799	275.6802	5.33E+16	67.09653	269.0373	215.4272
3	1 <sup>st</sup>	588	157.6672	6.42E+12	-5.37506	152.7785	155.9391
	2 <sup>nd</sup>	848.42	152.8455	43494411	-107.379	145.7918	236.8943
4	1 <sup>st</sup>	555.65	465.768	1.09E+43	573.8319	461.1483	142.2986
	2 <sup>nd</sup>	653.93	230.3459	1.21E+17	75.59674	224.9091	175.4742
	3 <sup>rd</sup>	823.77	184.2066	1.76E+10	-57.2209	177.3578	224.4946
5	1 <sup>st</sup>	569	221.2887	2.81E+19	122.0207	216.558	147.1282
	2 <sup>nd</sup>	795	181.4433	2.28E+10	-54.7908	174.8336	218.3923
6	1 <sup>st</sup>	544.75	84.64966	3120487	-125.6	80.12061	148.5412
	2 <sup>nd</sup>	766.18	1031.121	6.36E+69	1083.54	1024.751	194.5638
7	1 <sup>st</sup>	584.31	86.32033	1161066	-134.402	81.46237	159.9951
	2 <sup>nd</sup>	834.76	204.1593	2.01E+11	-37.0914	197.2191	228.1816
8	1 <sup>st</sup>	562.59	77.52232	477173.4	-141.48	72.84495	152.4404
	2 <sup>nd</sup>	640	180.8275	2.22E+13	4.22548	175.5065	172.8022
	3 <sup>rd</sup>	829.39	173.0599	2.1E+09	-74.9578	166.1644	228.3336

#### Structural and morphological characterization

Figures 3(a-d) depicts the X-ray diffraction patterns for Sc-complexes (5-8). The complexes (5-8) exhibit a well-defined XRD pattern with distinct peaks at 2θ (32 and 53°), (33, 58 and 65°), (32, 47, 58 and 65°) and (33, 49, 58 and 63°), respectively. These results are characteristic to crystalline Sc(III) metal that are in good agreement with references (JCPDS card no. 17-0714) [34]. The Debye-Scherrer equation [35] is utilized to determine the average crystallite sizes based on the values of full width at half maximum (FWHM) at 2θ reflections of the complexes (5-8). The average crystallite sizes range (22-69 nm). The Ostwald ripening theory can be used to assign the crystallite surface of complexes (5-8) [36]. An inhomogeneous structure changes over time to form bigger crystals or sol particles in the expense of small crystals or sol particles. This phenomenon is known as the Ostwald ripening theory, and it has been observed in both solid solutions and liquid sols [37]. Table 3 displays the dislocation network dislocation density (δ) and strain (ε) in the complexes. A low value for both strain and dislocation density indicates the creation of high-quality complexes [38].

Table 3. Physical data (2θ, intensity, d-spacing, crystallite sizes (D), dislocation density (δ) and strain (ε).

Complexes	2θ	Intensity	d-spacing	D (nm)	δ (10 <sup>12</sup> .lin.m <sup>-2</sup> )	ε (10 <sup>-4</sup> )
5	9.74	100	9.1440	69	0.0002	0.177
6	35.23	100	2.5462	22	0.0021	0.382

7	12	100	7.4128	42	0.0005	1.45
8	22.80	100	3.8750	28	0.0013	0.66

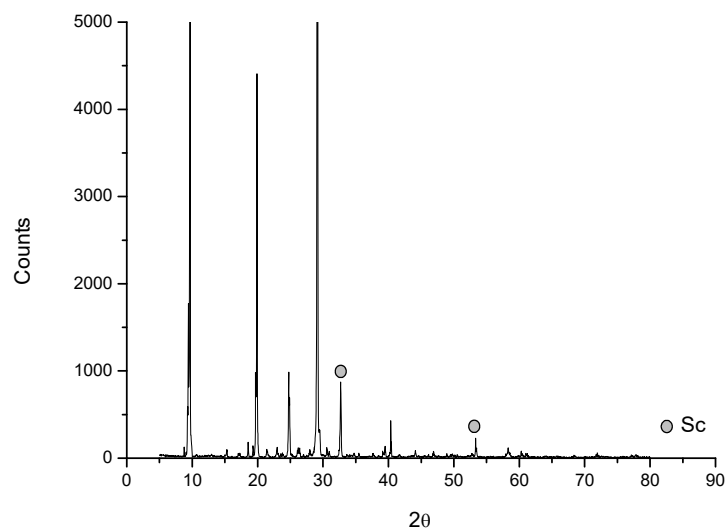


Figure 3a. XRD patterns of complex 5.

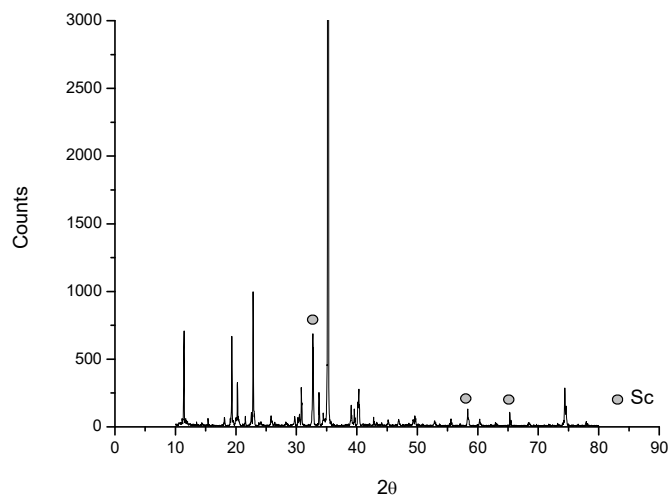


Figure 3b. XRD patterns of complex 6.

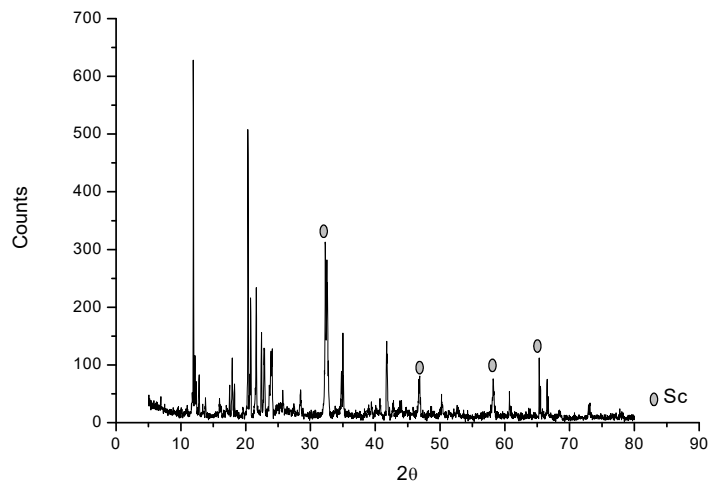


Figure 3c. XRD patterns of complex **7**.

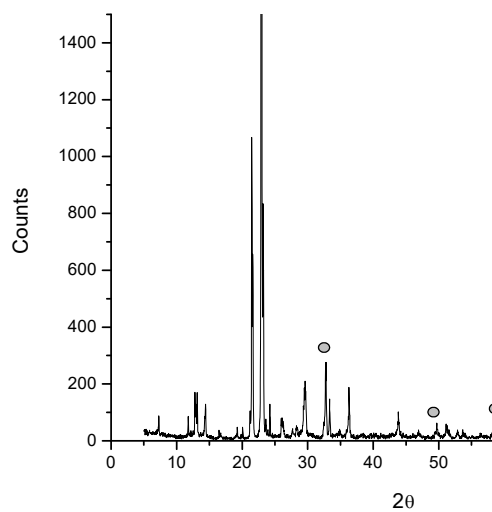


Figure 3d. XRD patterns of complex **8**.

Figures 4(a-d) display the SEM images of the four scandium(III)-complexes (5-8). Regarding images, the chelation comprises aggregated particles with homogeneous shape and distinct surfaces. The surface features of complexes **5** to **8** display significant enlargements, with magnifications of 4000, 500, 1000, and 1000 times, respectively. The corresponding drawing

scales are 5, 50, 10, and 10 $\mu$ m. Complex **5** appears stick-shaped with diameters that vary. The surface of complex **6** exhibits a staircase pattern resembling a ladder, while complex **7** takes the form of small spherical pellets with different diameters. On the other hand, the surface of complex **8** resembles crushed snow.

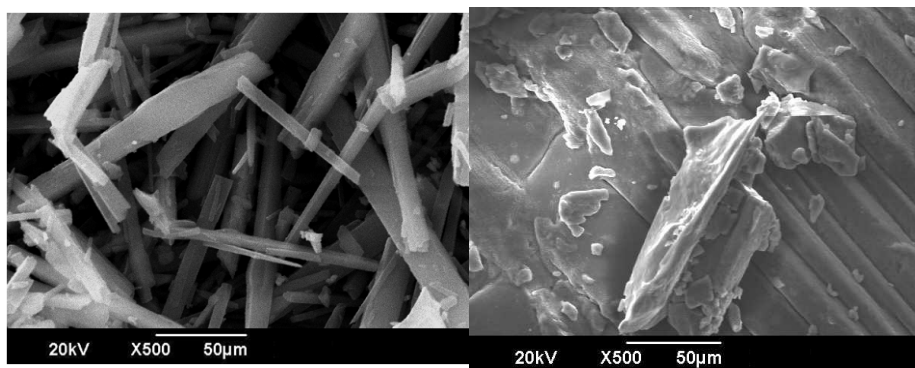


Figure 4a. SEM morphology of compound **5**.

Figure 4b. SEM morphology of compound **6**.

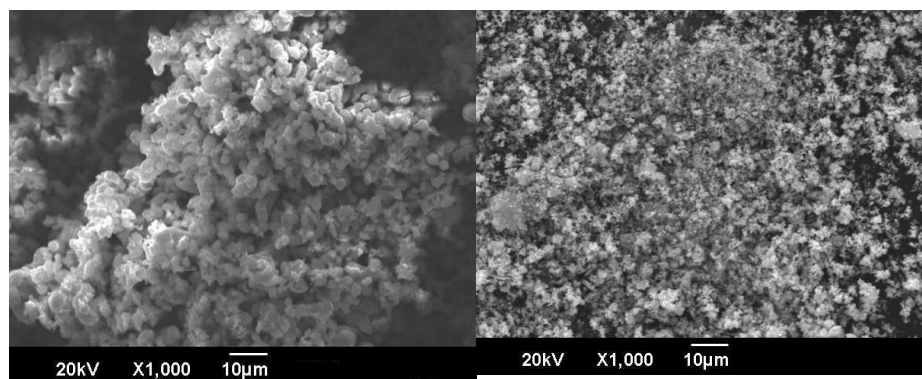


Figure 4c. SEM morphology of compound **7**.

Figure 4d. SEM morphology of compound **8**.

Figures 5(a-d) of the TEM micrographs reveal nanoparticles for complexes **5** to **8**, exhibiting a nanosized morphology. The average diameter of the particles in complexes **5** to **8** was determined by fitting the TEM data to a normal distribution. Analysis of the images indicates that the particle sizes range from 20 nm to 100 nm. The TEM micrographs in Figures 5(a-d) display dark spots of spherical or stick-like shapes, varying in size. Complex **6** particularly demonstrates a nanosized structure that closely corresponds to the XRD spectrum, suggesting that its size and shape are influenced by aggregation [39].

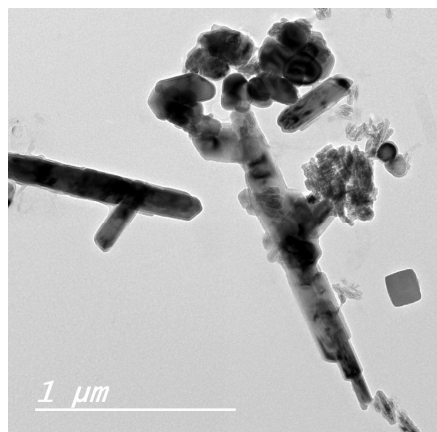


Figure 5a. TEM morphology of complex 5.

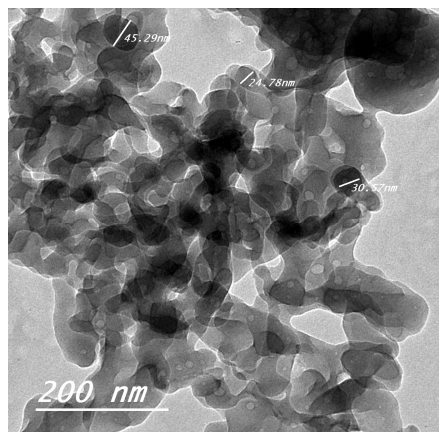


Figure 5b. TEM morphology of complex 6.

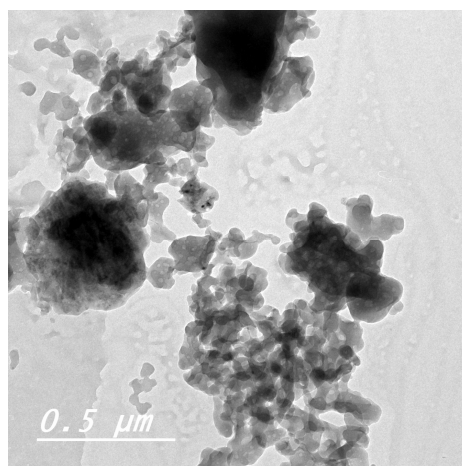


Figure 5c. TEM morphology of complex 7.

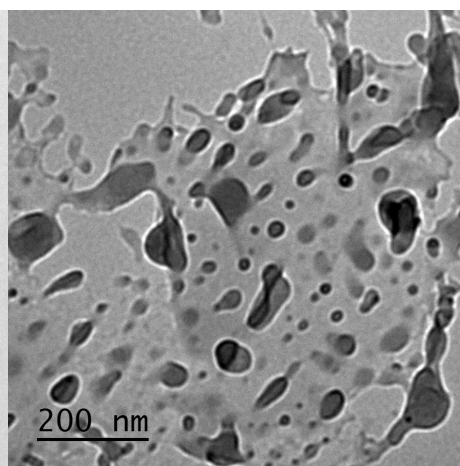


Figure 5d. TEM morphology of complex 8.

#### Computational calculations

Using the density functional theory (DFT) method, the molecular modelling was created structures 1-24 and several energetic parameters were estimated, including bond length, bond angle, chemical reactivity, MEP, total energy, dipole moment, and binding energy for sulf-1(1), sulf-2(2), sulf-3(3), sulf-4(4), [Sc(sulf-1)<sub>2</sub>(Cl)<sub>2</sub>](5), [Sc(sulf-2)<sub>2</sub>(Cl)<sub>2</sub>](6), [Sc(sulf-3)<sub>2</sub>(Cl)<sub>2</sub>](7), and [Sc(sulf-4)<sub>2</sub>(Cl)<sub>2</sub>](8). Furthermore, the following conclusions have been drawn from the tabulated data: 1) Complexation causes a bit of a difference in the bond lengths of the compound moieties (1-4) [40]. They are either decreased or increased; the most substantial change is triggered in the (N-S) sulphonamido groups in compounds (5-8). However, (N-C) bonds either elongated as in compound (5), or shortened as in compounds 6, 8. The new Sc-N bonds either shortened to indicate the higher strength of Sc-N bonds or elongated. The coordinate bonds between Sc and Nitrogen-sulphonamido groups are shorter than other coordinate bonds. Sc(3)-

N(21, 25) bonds in compound **6** are the shortest indicating the higher bond strength, followed by Sc(35)-N(25, 26), Sc(39)-N(25, 26) and Sc(11)-N(36, 37) in compounds **8**, **6** and **7**, respectively. 2) The bond angles in all compounds **5-8** are fairly close to tetragonal geometry, which predicts  $sp^3d^2$  or  $d^2sp^3$  hybridization [27]. 3) Equations 9–13 were used to calculate the energies of the frontier molecular orbitals ( $E_{HOMO}$ ,  $E_{LUMO}$ ), electronegativity ( $\chi$ ), chemical potential ( $\mu$ ), global softness ( $S$ ), global hardness ( $\eta$ ), global electrophilicity index ( $\omega$ ), and energy band gap, which explains the molecule's inevitable charge exchange cooperation [41-43]. The results are displayed in Table 4.

$$\chi \text{ (electronegativity)} = -\frac{1}{2} (E_{LUMO} + E_{HOMO}) \quad (9)$$

$$\mu \text{ (potential)} = -\chi = \frac{1}{2} (E_{LUMO} + E_{HOMO}) \quad (10)$$

$$\eta \text{ (hardness)} = \frac{1}{2} (E_{LUMO} - E_{HOMO}) \quad (11)$$

$$S \text{ (softness)} = \frac{1}{2} \eta \quad (12)$$

$$\omega \text{ (electrophilicity)} = \frac{\mu^2}{2\eta} \quad (13)$$

$$\sigma = 1/\eta \quad (14)$$

According to data reported in Tables 4, 5, i) A compound's gas phase energy declines as its molecular weight rises. ii) The stability of the investigated compounds is shown by the -ve sign of the computed energy parameters [44]. iii) According to frontier orbital theory, a molecule's capacity to donate electrons to a lower LUMO energy is improved by a greater HOMO energy [45]. Compounds (**1-4**) have a strong tendency to coordinate metal ions due to their tiny energy band gap, particularly because the HOMO level is primarily localised on the nitrogen atoms of sulphamido and anilino groups [42]. The narrow energy gap for the sulfa drugs, facilitates the flow of charge and consequently this can be used in biological as well as solar cells applications.  $\Delta E_{H-L}$  for compounds (**5-8**) are relatively higher than the corresponding compounds (**1-4**). Furthermore, the kinetic stability and chemical reactivity of compounds can be described using the stability index that tiny  $\Delta E_{H-L}$  values. iv) Quantifying the stability and reactivity of molecules requires knowledge of global softness ( $S$ ) and global hardness ( $\eta$ ). Compared to a hard molecule, a soft molecule has a smaller energy gap. When forming a complex, the drug ligand acts as a Lewis base and the metal ion as a Lewis acid. The correct value ( $S$ ) controls the degree of softness and hardness of species, therefore, soft acid is the best choice for complexation with soft base ligands [43]. The computed chemical potential ( $\mu$ ) supports this as well. v) The electrophilicity index ( $\omega$ ) [44] also accurately measures the biological activity of drug receptor contact, in addition to the electrical charge that a system absorbs from its environment, which causes energy stabilization. vi) The total energy, binding energy, and dipole moment were outlined in Tables 5. The computed binding energy for the compounds (**5-8**) is higher and more stable than the compounds (**1-4**).

Table 4. The energy parameters for compounds (**1-8**) calculated by DMOL<sup>3</sup> using DFT- method.

Compound	-EH/ eV	-EL/ eV	-EH-EL/ eV	$\chi$ / eV	$\mu$ / eV	$\eta$ / eV	S/ eV <sup>-1</sup>	$\omega$ / eV	$\sigma$ / eV <sup>-1</sup>
(1)	5.114	1.512	3.602	3.313	-3.313	0.9005	0.4502	6.0943747	1.11049
(2)	5.032	1.321	3.711	3.176	-3.1765	0.92775	0.4639	5.4379694	1.07788
(3)	4.716	1.781	2.935	3.248	-3.2485	0.73375	0.3669	7.1909725	1.36286
(4)	4.690	1.941	2.749	3.315	-3.3155	0.68725	0.3436	7.9974829	1.45507
(5)	5.466	2.000	3.466	3.733	-3.733	0.8665	0.4332	8.0411361	1.15407
(6)	5.634	1.972	3.662	3.803	-3.803	0.9155	0.4577	7.8988580	1.0923
(7)	5.507	2.259	3.248	3.883	-3.883	0.812	0.4060	9.2842912	1.23153
(8)	5.029	4.031	0.998	4.530	-4.53	0.2495	0.1247	41.124048	4.00802

Table 5. Some energetic parameters of compounds (**1-8**) calculated by DMOL<sup>3</sup> using DFT- method.

Compound	Total energy (kcal/mol)	Binding energy (kcal/mol)	Dipole moment (D)
(1)	-7.75E+05	-3.93E+03	14.4267
(2)	-5.60E+05	-2.00E+03	11.4533
(3)	-7.38E+05	-3.22E+03	21.3782
(4)	-7.25E+05	-3.21E+03	12.5832
(5)	-2.17E+06	-8.26E+03	14.0478
(6)	-1.73E+06	-4.60E+03	14.9616
(7)	-2.09E+06	-6.85E+03	11.4410
(8)	-2.07E+06	-6.82E+03	8.5665

#### Molecular electrostatic potential (MEP)

The molecular electrostatic potential (MEP) represents a representation of the electrostatic potential  $V(r)$  at a specific point  $r(x, y, z)$  projected onto a surface with a constant electron density. It is a valuable tool for investigating molecular structure and understanding its physicochemical properties [46-49]. The nitrogen atoms have regions of negative potential with high negative values;  $N(19) = -0.726$ ,  $N(1) = -0.889$ ,  $N(8) = -0.693$ , and  $N(2) = -681$  for compounds **1**, **2**, **3**, and **4**, respectively) however, the regions above the hydrogen and carbon atoms (the high positive values belong to  $C(12) = +0.569$ ,  $C(3) = +0.483$ ,  $C(2) = +0.727$ ,  $C(12) = +0.670$  for compounds **1**, **2**, **3** and **4**, respectively).

#### Vibrational calculation for sulf drugs

Experiments were performed on solid samples, although for compounds **1-4** frequency calculations were performed on the free drug in a vacuum. Consequently, the vibrational wavenumbers show a small discrepancy between the experiments and theory. The complicated nature of the vibrational modes is mostly caused by the ligands' low symmetry. It is difficult to assign vibrations in the plane, out of plane, and torsional modes because they frequently interact with substituent and ring modes [49]. Still, the infrared (IR) spectrum has several prominent frequencies that are useful for characterisation. The following equations describe the linear relationships that are seen for both ligands between the calculated and experimental wavenumbers:

For the (**1**):  $\nu_{\text{cal}} = 1.00143 \nu_{\text{Exp}} - 4.53664$  with  $R^2 = 0.99996$ .

For the (**2**):  $\nu_{\text{cal}} = 1.00422 \nu_{\text{Exp}} - 15.32552$  with  $R^2 = 0.99994$ .

For the (**3**):  $\nu_{\text{cal}} = 0.99799 \nu_{\text{Exp}} - 2.73852$  with  $R^2 = 0.99994$ .

For the (**4**):  $\nu_{\text{cal}} = 0.99622 \nu_{\text{Exp}} - 4.08687$  with  $R^2 = 0.99998$ .

## CONCLUSION

Four types of sulfa drugs, namely sulfadimidine (**1**), sulfanilamide (**2**), sulfamethoxazole (**3**), and sulfadiazine (**4**), were employed to synthesize four scandium(III) complexes of sulfa drugs. These complexes are denoted as  $[\text{Sc}(\text{sulf-1})_2(\text{Cl})_2]\text{Cl}$  (**5**),  $[\text{Sc}(\text{sulf-2})_2(\text{Cl})_2]\text{Cl}$  (**6**),  $[\text{Sc}(\text{sulf-3})_2(\text{Cl})_2]\text{Cl}$  (**7**), and  $[\text{Sc}(\text{sulf-4})_2(\text{Cl})_2]\text{Cl}$  (**8**). Further techniques have been studied as a complementary work as the thermal, kinetic, morphological and computational investigations. The compounds (**5-8**) were prepared by 1:2 molar ratios between scandium(III) chloride and compounds (**1-4**). TG curves have been examined for the compounds to determine their kinetic and thermodynamic

functions using approaches. The X-ray powder diffraction (XRD) patterns support the crystalline appearance of compounds (**5-8**). The nano-sized structure, the surface morphology as well as the morphology of particles were studied by scanning electron microscopy (SEM) and transmission electron microscopy (TEM) techniques. Additionally, the bond angles observed in the complexes provide insight into the octahedral coordination environment surrounding the Sc(III) ions, suggesting the possibility of  $sp^3d^2$  or  $d^2sp^3$  hybridization. The disparities between the theoretical and experimental IR frequencies can be attributed to variations in the measurement phases or conditions. Other energy parameters were computed using DFT method.

### ACKNOWLEDGEMENTS

Princess Nourah bint Abdulrahman University Researchers Supporting Project number (PNURSP2025R75), Princess Nourah bint Abdulrahman University, Riyadh, Saudi Arabia.

### REFERENCES

1. Supuran, C.T.; Mincione, F.; Scozzafava, A.; Briganti, F.; Mincione, G.; Ilies, M.A. Carbonic anhydrase inhibitors - Part 52. Metal complexes of heterocyclic sulfonamides: A new class of strong topical intraocular pressure-lowering agents in rabbits, *Eur. J. Med. Chem.* **1998**, *33*, 247-254.
2. Abd El-Wahed, M.G.; Refat, M.S.; El-Megharbel, S.M. Spectroscopic, thermal and biological studies of the coordination compounds of sulfasalazine drug: Mn(II), Hg(II), Cr(III), ZrO(II), VO(II) and Y(III) transition metal complexes. *Chem. Pharm. Bull.* **2008**, *56*, 1585-1591.
3. Refat, M.S.; Mohamed, S.F. Spectroscopic, thermal and antitumor investigations of sulfasalazine drug in situ complexation with alkaline earth metal ions, *Spectrochim. Acta A* **2011**, *82*, 108-117.
4. Abd El-Wahed, M.G., El-Megharbel, S.M.; El-Sayed, M.Y.; Zahran, Y.M.; Refat, M.S. Synthesis and characterization of some lanthanide metal complexes Ce(III), Gd(III), Nd(III), Tb(III), and Er(III) with sulfasalazine as sulfa drug. *Bulg. Chem. Commun.* **2015**, *47*, 895-903.
5. Hassan, M.; Nasr, S.M.; Abd-El Razek, S.E.; Abdel-Aziz, M.S.; El-Gamasy, S.M. New superior bioactive metal complexes of ligand with N, O donor atoms bearing sulfadiazine moiety: Physicochemical study and thermal behavior for chemotherapeutic application. *Arab. J. Chem.* **2020**, *13*, 7324-7337.
6. Rostamizadeh, S.; Daneshfar, Z.; Moghimi, H. Synthesis of sulfamethoxazole and sulfabenzamide metal complexes; evaluation of their antibacterial activity. *Eur. J. Med. Chem.* **2019**, *171*, 364-371.
7. Bouchoucha, A.; Zaater, S.; Bouacida, S.; Merazig, H.; Djabbar, S. Synthesis and characterization of new complexes of nickel(II), palladium(II), and platinum(II) with derived sulfonamide ligand: Structure, DFT study, antibacterial, and cytotoxicity activities. *J. Mol. Struct.* **2018**, *1161*, 345-355.
8. Al-Khodir, F.A.I. Ca(II), Zn(II), and Au(III) sulfamethoxazole sulfa-drug complexes: Synthesis, spectroscopic, and anticancer evaluation studies. *Orient. J. Chem.* **2015**, *31*, 1277-1285.
9. Saad, F.A. Elaborated molecular docking and DFT/B3LYP studies for novel Sulfa drug complexes, spectral and antitumor investigations. *J. Therm. Anal. Calorim.* **2017**, *129*, 425-440.
10. Sharfalddin, A.A.; Emwas, A.-H.; Jaremko, M.; Hussien, M. A. Practical and computational studies of bivalence metal complexes of sulfaclozine and biological studies. *Front. Chem.* **2021**, *9*, 644691.

11. Hassan, A.U.; Sumrra, S.H.; Imran, M.; Chohan, Z.H. New 3D multifunctional metal chelates of sulfonamide: spectral, vibrational, molecular modeling, DFT, medicinal, and in silico studies. *J. Mol. Struct.* **2022**, 1254, 132305.
12. Shehnaz; Siddiqui, W.A.; Raza, M.A.; Ashraf, A.; Ashfaq, M.; Tahir, M.N.; Niaz, S. Structure elucidation {single X-ray crystal diffraction studies, hirshfeld surface analysis, DFT} and antibacterial studies of sulfonamide functionalized Schiff base copper(II) and zinc(II) complexes. *J. Mol. Struct.* **2024**, 1295, 136603.
13. Selçuki, N.A.; Coşkun, E.; Biçer, E. Combined computational and experimental studies on cysteine-sulfadiazine adduct formation. *Turk. J. Chem.* **2020**, 44, 343-356.
14. Al-Hawarin, J.I.; Abu-Yamin, A.-A.; Abu-Saleh, A.A.A.; Saraireh, I.A.M.; Almatarneh, M. H.; Hasan, M.; Atrooz, O.M.; Al-Douri, Y. Synthesis, characterization, and DFT calculations of a new sulfamethoxazole Schiff Base and its metal complexes. *Matsl.* **2023**, 16, 5160.
15. Bouzaheur, A.; Bouchoucha, A.; Larbi, K.S.; Zaater, S. Experimental and DFT studies of a novel Schiff base sulfonamide derivative ligand and its palladium(II) and platinum(IV) complexes: Antimicrobial activity, cytotoxicity, and molecular docking study. *J. Mol. Struct.* **2022**, 1261, 132811.
16. Varshney, A.; Mishra, A.P. Synthesis, spectral characterization, computational studies, antifungal, DNA interaction, antioxidant, and fluorescence property of novel Schiff base ligand and its metal chelates. *Spectrochim. Acta A* **2023**, 297, 122765.
17. Jamil, Y.M.; Al-Maqtari, M.A.; Al-Qadasi, M.K. Ligational and spectroscopic studies on some sulfamethoxazole metal complexes as antimicrobial agents. *Eur. J. Pharm. Med. Res.* **2017**, 4, 95-105.
18. Öztürk, F. Structural characterization (XRD, FTIR) and magnetic studies of Cd(II)-sulfamethoxazole-2,2'-bipyridine: DFT and hirshfeld surface analysis. *J. Mol. Struct.* **2023**, 1271, 133945.
19. Bourouai M.A.; Larbi K.S.; Bouchoucha A.; Terrachet-Bouaziz S.; Djebbar S.; New Ni(II) and Pd(II) complexes bearing derived sulfa drug ligands: Synthesis, characterization, DFT calculations, and in silico and in vitro biological activity studies. *Biometals* **2023**, 36, 153-188.
20. Refat, M.S.; El-Habeeb, A.A. Synthesis, spectroscopic and antimicrobial investigations of scandium(III) complexes with four kinds of sulfa drugs. *Spectrosc. Spectr. Anal.* **2020**, 40, 985-990.
21. Kessi, A.; Delley, B. Density functional crystal vs. cluster models as applied to zeolites. *Int. J. Quantum Chem.* **1998**, 68, 135-144.
22. Delley, B. A scattering theoretic approach to scalar relativistic corrections on bonding. *Int. J. Quantum Chem.* **1998**, 69, 423-433.
23. Delley, B. From molecules to solids with the DMol3 approach. *J. Chem. Phys.* **2000**, 113, 7756-7764.
24. Hammer, B.; Hansen, L.B.; Nørskov, J.K. Improved adsorption energetics within density functional theory using revised Perdew-Burke-Ernzerhof functionals. *Phys. Rev. B* **1999**, 59, 7413-7421.
25. Coats, A.; Redfern, J. Thermogravimetric analysis: A review. *Nature* **1964**, 201, 68-69.
26. Horowitz, H.H.; Metzger, G. A new analysis of thermogravimetric traces. *Anal. Chem.* **1963**, 35, 1464-1468.
27. Taakeyama, T.; Quinn, F.X. *Thermal Analysis: Fundamentals and Applications to Polymer Science*. John Wiley and Sons: Chichester; **1994**.
28. Mano, J.F.; Koniarova, D.; Reis, R.L. Thermal properties of thermoplastic starch/synthetic polymer blends with potential biomedical applicability. *J. Mater. Sci. Mater. Med.* **2003**, 14, 127-135.
29. Moore, J.W.; Pearson, R.G. *Kinetics and Mechanism*. John Wiley and Sons: New York; **1961**.

30. Maravalli, P.B.; Goudar, T.R. Thermal decomposition kinetics of some coordination compounds. *Thermochim. Acta* **1999**, *35*, 235-242.
31. Kandil, S.S.; El-Hefnawy, G.B.; Baker, E.A. Thermal and spectral studies of 5-(phenylazo)-2-thiohydantoin and 5-(2-hydroxyphenylazo)-2-thiohydantoin complexes of cobalt(II), nickel(II), and copper(II). *Thermochim. Acta* **2004**, *414*, 105-112.
32. El-Gammal, O.A. Spectroscopic and thermal studies on some metal complexes of a novel Schiff base ligand. *Spectrochim. Acta A* **2010**, *75*, 533-542.
33. Nawar, N.; Mostafa, M.M.; Al-Radadi, N.S. Synthesis, characterization, and biological activity of some transition metal complexes with a novel Schiff base ligand. *Open J. Inorg. Chem.* **2016**, *6*, 23-65.
34. Harata, M.; Nakamura, T.; Yakushiji, H.; Okabe, T.H. Mineral processing and extractive metallurgy. *Miner. Process. Extr. Metall.* **2008**, *117*, 95-101.
35. Klug, H.P.; Alexander, L.E. *X-Ray Diffraction Procedures for Polycrystalline and Amorphous Materials*. Wiley: New York; **1974**.
36. Hansen, T.W.; DeLaRiva, A.T.; Challa, S.R.; Datye, A.K. Sintering of catalytic nanoparticles: Particle migration or ostwald ripening? *Acc. Chem. Res.* **2013**, *46*, 1720-1730.
37. IUPAC *Compendium of Chemical Terminology*, 2nd ed. (the "Gold Book"). Blackwell Scientific Publications: Oxford; **1997**.
38. Velumani, S.; Mathew, X.; Sebastian, P.J. Synthesis and characterization of CuInS<sub>2</sub> thin films for solar cell applications. *Sol. Energy Mater. Sol. Cells* **2003**, *76*, 359-368.
39. Carotenuto, G.; Nicolais, F. Synthesis and characterization of metal-polymer nanocomposites. *Mats.* **2009**, *2*, 1323-1340.
40. Despaigne, A.A.R.; Da Silva, J.G.; Do Carmo, A.C.M.; Piro, O.E.; Castellano, E.E.; Beraldo, H. Copper(II) and zinc(II) complexes with 2-benzoylpyridine-methyl hydrazone. *J. Mol. Struct.* **2009**, *920*, 97-102.
41. El-Sherif, A.A.; Fetoh, A.; Abdulhamed, Y.Kh.; Abu El-Reash, G.M. Synthesis, structural characterization, DFT studies, and biological activity of Cu(II) and Ni(II) complexes of novel hydrazone. *Inorg. Chim. Acta* **2018**, *480*, 1-15.
42. El-Reash, G.A.; El-Gammal, O.; Ahmed, F. Molecular structure and biological studies on Cr(III), Mn(II), and Fe(III) complexes of heterocyclic carbohydrazone ligand. *Spectrochim. Acta A* **2014**, *121*, 259-267.
43. Yousef, T.A.; Abu El-Reash, G.M.; El Morshedy, R.M. Quantum chemical calculations, experimental investigations, and DNA studies on (e)-2-((3-hydroxynaphthalen-2-yl)methylene)-n-(pyridin-2-yl)hydrazinecarbothioamide and its Mn(II), Ni(II), Cu(II), Zn(II), and Cd(II) complexes. *Polyhedron* **2012**, *45*, 71-85.
44. Parthasarathi, R.; Padmanabhan, J.; Subramanian, V.; Sarkar, U.; Maiti, B.; Chattaraj, P. Toxicity analysis of benzidine through chemical reactivity and selectivity profiles: A DFT approach. *Internet Electron. J. Mol. Des.* **2003**, *2*, 798-813.
45. Kandil, S.S.; El-Hefnawy, G.B.; Baker, E.A. Thermal and spectral studies of 5-(phenylazo)-2-thiohydantoin and 5-(2-hydroxyphenylazo)-2-thiohydantoin complexes of cobalt(II), nickel(II), and copper(II). *Thermochim. Acta* **2004**, *414*, 105-112.
46. Sagdinc, S.; Koksoy, B.; Kandemirli, F.; Bayari, S.H. Theoretical and spectroscopic studies of 5-fluoro-isatin-3-(n-benzylthiosemicarbazone) and its zinc(II) complex. *J. Mol. Struct.* **2009**, *63*, 917-923.
47. Luque, F.J.; López, J.M.; Orozco, M. Perspective on electrostatic interactions of a solute with a continuum. A direct utilization of ab initio molecular potentials for the prevision of solvent effects. *Theor. Chem. Acc.* **2000**, *103*, 345-350.
48. Okulik, N.; Jubert, A.H. Theoretical analysis of the reactive sites of non-steroidal anti-inflammatory drugs. *Internet Electron. J. Mol. Des.* **2005**, *4*, 17-30.

49. Lu, Y.; Wang, Y.; Jiang, Z.; Men, Y. Molecular weight dependency of surface free energy of native and stabilized crystallites in isotactic polypropylene. *ACS Macro Lett.* **2014**, *3*, 1101-1105.